

Article

Electrochemical Sodium Ion Sensor Based on Silver Nanoparticles/Graphene Oxide Nanocomposite for Food Application

Pranlekha Traiwatcharanon ¹, Wilai Siriwatcharapiboon ² and Chatchawal Wongchoosuk ^{1,*} 

¹ Department of Physics, Faculty of Science, Kasetsart University, Bangkok 10900, Thailand; t.pranlekha@gmail.com

² Department of Chemistry and Center of Excellence for Innovation in Chemistry, Faculty of Science, Kasetsart University, Bangkok 10900, Thailand; fsciwls@ku.ac.th

* Correspondence: chatchawal.w@ku.ac.th; Tel.: +662-562-5555

Received: 4 June 2020; Accepted: 25 July 2020; Published: 28 July 2020



Abstract: High sodium ion (Na^+) consumption leads to high blood pressure which causes many health issues. Real-time determination of Na^+ content in food is still important to limit Na^+ intake and control the taste of food. In this work, we have developed an electrochemical sensor based on agglomeration of silver nanoparticles (AgNPs) and graphene oxide (GO) modified on a screen-printed silver electrode (SPE) for Na^+ detection at room temperature by using cyclic voltammetry (CV). The AgNPs were synthesized through a simple green route using *Pistia stratiotes* extract as a reducing agent under blue light illumination and mixed with the GO to be a Na^+ selective sensing nanocomposite. The AgNPs/GO/SPE sensor showed high sensitivity (0.269 mA/mM/cm^2), high selectivity, linear relationship (0–100 mM), good stability, and excellent reproducibility to Na^+ detection as well as low limit of detection (9.344 mM) for food application. The interfering species such as K^+ , Zn^{2+} , Na^+ , Mg^{2+} , glucose, and ascorbic acid did not have any influence on the Na^+ determination. The AgNPs/GO/SPE sensor was successfully applied to determine Na^+ in real samples such as fish sauce and seasoning powder of instant noodle.

Keywords: AgNPs; graphene oxide; AgNPs/GO; electrochemical sensor; sodium ion detection; sensor for food application; salt estimation

1. Introduction

Sodium ion (Na^+) is an essential element in human body for regulating body's fluids balance and maintaining the responses of nerves and muscles normally [1]. The main source of Na^+ is salt in foods. Based on clinical trials, the recommendation for Na^+ intake in the adult should be below 100 mmol (~2.3 g of Na^+ or 5.8 g of salt) per day [2,3]. However, most people in many countries consume excess level of Na^+ which is about twice as much as the body needs [4,5]. The excess Na^+ consumption causes high blood pressure and increases the risk of cardiovascular disease, heart disease, and stroke [6–8]. Therefore, real-time determination of Na^+ content in food is still important to limit Na^+ intake, control hypertension and lower health issues as well as the standardization of food taste.

The most common methods for determination of Na^+ in foods are based on spectroscopic techniques such as flame atomic absorption/emission spectrometry, inductively coupled plasma spectroscopy, infrared enthalpymetric method, liquid chromatography, and ion mobility spectrometry [9,10]. Although these techniques can identify the Na^+ content in foods with high accuracy and precision, they required the use of expensive instrument with complicated results. Currently, ion sensitive field-effect transistors (ISFETs) become one of the potential methods for real-time Na^+ detection.

For example, Garcia-Cordero et al. [11] fabricated an ISFET integrated with microfluidic interface for real-time measurement of Na^+ and K^+ from sweat. Lu et al. [12] developed single HfO_2 gate ISFETs with and without CF_4 plasma treatment to monitor Na^+ and K^+ with linear response. Cazalé et al. [13] presented the preparation of N-channel $\text{SiO}_2/\text{Si}_3\text{N}_4$ -gate ISFET microsensors for analysis of sweat samples with low pH interferences. Zhang et al. [14] reported the development of 3D-extended-metal-gate ISFETs to high sensitive towards pH and multiple ions (Na^+ , K^+ , and Ca^{2+}) in vitro real sweat tests. However, the fabrication of high performance ISFETs requires complicated process and high advance technologies. An alternative approached for Na^+ determination could be done via normal electrochemistry based on modified printed electrodes that have intensive interest due to their rapidity, simplicity, portability, and low-cost. The high sensitivity and selective working electrode to the target analyte is an important key for development of electrochemical sensor. Several nanomaterials including carbon-based nanomaterials, metal nanoparticles, and nanocomposites have been used to modify a surface of working electrode for detection of food additives and contaminants such as hydrazine, malachite green, bisphenol A, ascorbic acid, caffeine, nitrite, etc. [15].

A nanocomposite between silver nanoparticles (AgNPs) and graphene oxide (GO) has been received an interest in surface modification of the working electrode for Na^+ detection in this work. The AgNPs were found to have biocompatibility, high free-radical generation, low toxicity, and good electrocatalytic activity [16,17] while GO exhibited large surface area and excellent electronic properties [18–22]. The GO incorporated with AgNPs nanocomposite is believed to be an excellent candidate material for high sensitivity to Na^+ in food application. In this work, we aimed to develop disposable electrochemical sensor based on AgNPs/GO nanocomposite modified on screen-printed silver electrode (SPE) for Na^+ determination at room temperature by using cyclic voltammetry (CV). The AgNPs/GO nanocomposite was prepared by simple and low-cost method through a green route synthesis. The conditions influencing determination of Na^+ were optimized. The AgNPs/GO/SPE sensor was subsequently used for determination of Na^+ in fish sauce and seasoning powder of instant noodles.

2. Materials and Methods

2.1. Chemicals

Ethylene glycol (EG), sodium hydroxide (NaOH), silver nitrate (AgNO_3), zinc chloride (ZnCl_2), D-(+) glucose ($\text{C}_6\text{H}_{12}\text{O}_6$), magnesium sulfate (MgSO_4), ethanol ($\text{C}_2\text{H}_4\text{O}$), hydrochloric acid (HCl), and tris(hydroxymethyl)aminomethane (TRIS) were purchased from Sigma-Aldrich. L-ascorbic acid ($\text{C}_6\text{H}_8\text{O}_6$) was purchased from Tokyo chemical industry (TCI). Potassium chloride was purchased from Carlo erba reagents. All chemicals were analytical grade and used without further purification. The supporting electrolyte for all studies was a 0.1 M of TRIS solution. It should be noted that the pH 10 is achieved after adding of TRIS solution. The pH can be adjusted from pH 10 to pH 4 by additions of dilute HCl. A Na^+ stock solution was prepared and used for preparing different concentrations of Na^+ solution in a range of 0–100 mM.

2.2. Synthesis of AgNPs and AgNPs/GO Nanocomposite

AgNPs were synthesized by a green route method as shown in Figure 1. Firstly, the small pieces of fresh *Pistia stratiotes* L. leaves were rinsed thoroughly with deionized water to remove dust particles from the biomass and dried in the clean air at the room temperature. Then, 50 g of the *Pistia stratiotes* L. leaves were put in a beaker containing 300 mL of deionized water and boiled for 20 min. After cooling down to room temperature, the extract solution was filtered through Whatman filter paper. 10 mL of *Pistia stratiotes* L. extract was then added into 10 mL of 10 mM AgNO_3 solution. The pH of the mixture was adjusted to pH 10 by addition of NaOH. The blue light irradiation was applied to the mixture under stirring for the reduction process of Ag^+ to Ag^0 at room temperature. The complete reaction for AgNPs formation was monitored by the change in color of the mixture from yellowish to deep brown.

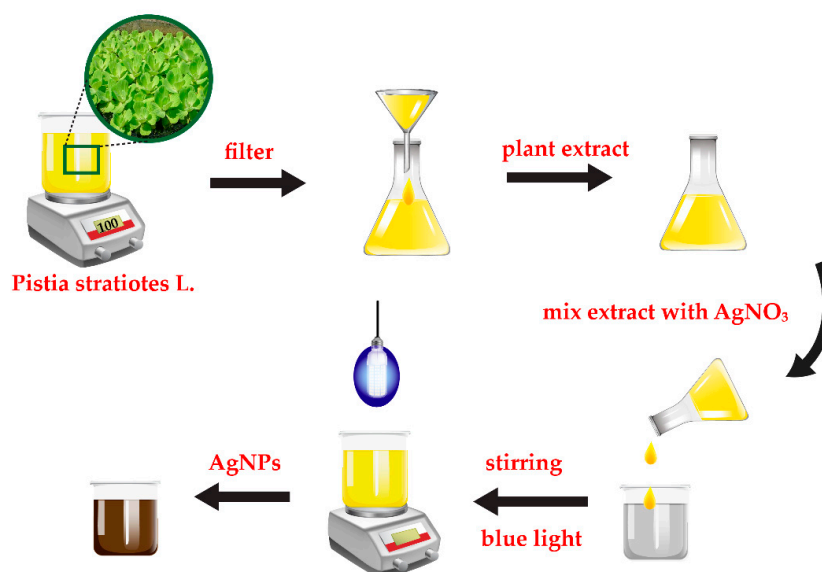


Figure 1. Schematic diagram of silver nanoparticles (AgNPs) synthesis based on a green route method.

GO was prepared by a chemical vapor deposition process [23]. In brief, GO was grown on copper foil by using mixture of hydrogen and methane as a carbon source. GO was synthesized at 1000 °C for 30 min. After obtaining GO powder, 3 mg of GO was dispersed in the EG (4 mg/mL concentration) and sonicated for 1 h. Subsequently, 1 M NaOH solution was added into the GO solution and sonicated for 30 min. 10 mL of AgNPs solution was then added dropwise to the mixture and sonicated again for 30 min to get a homogeneous AgNPs/GO nanocomposite as shown in Figure 2.

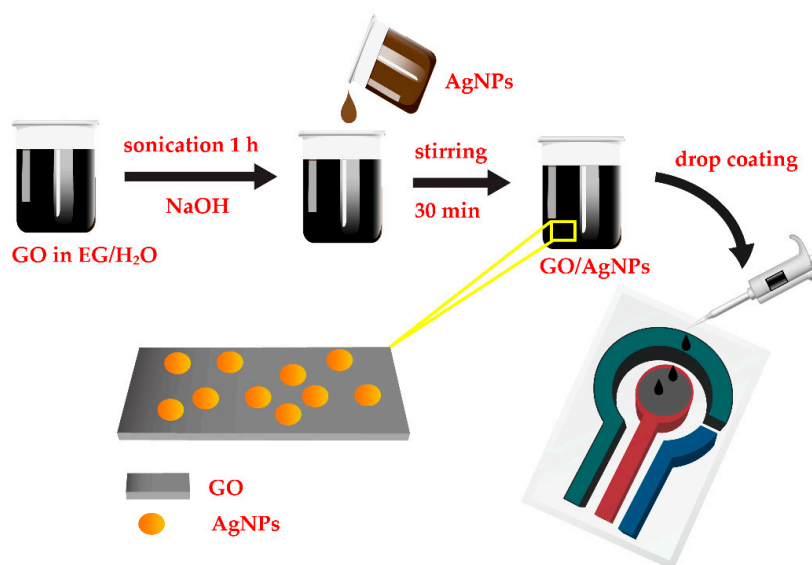


Figure 2. Schematic diagram of preparation of AgNPs/graphene oxide (GO) nanocomposite and fabrication of AgNPs/GO/SPE (screen-printed silver electrode) sensor for Na⁺ detection.

2.3. Fabrication and Measurement of AgNPs/GO/SPE Sensor

The synthesized AgNPs/GO nanocomposite was used as sensing nanomaterial for Na⁺ detection. 5 μL of AgNPs/GO nanocomposite suspension was drop-casted on the working electrode (7.065 mm² area) of SPE dried at 30 °C as shown in Figure 2. The SPEs purchased from Quasense consist of a silver working electrode, a carbon counter electrode and an Ag/AgCl reference electrode. The sensing performance of AgNPs/GO/SPE sensors were investigated via CV measurements. The voltammetric

measurements were performed with an EmStat Pico module potentiostat (PalmSens BV) controlled by PSTrace software. The CV measurements were obtained in a potential range between -1.0 V and $+1.0$ V vs. Ag/AgCl at 100 mV s^{-1} in 0.1 M TRIS solution. The electrochemical measurements were repeated for three times. The morphologies of the AgNPs/GO were characterized by transmission electron microscopy (TEM, JEM-3100F) and scanning electron microscope (SEM, SU8030-Hitachi). The absorption behavior of AgNPs/GO was examined by UV-Vis spectrophotometry (PerkinElmer Lambda-650). Raman spectrum was operated with the laser excitation wavelength of 785 nm by using a Raman spectroscopy (Renishaw model: Invia).

2.4. Chronoamperometric Measurement of AgNPs/GO/SPE Sensor

To evaluate the selectivity of AgNPs/GO/SPE sensors, they were examined by the chronoamperometry (CA) method which is a method for measuring the relationship between response current with time. The electrode was subjected to chronoamperometry with an applied potential of $+0.2$ V for 420 s with the addition of each interference for every 60 s. The interfering compounds included K^+ , Zn^{2+} , Na^+ , Mg^{2+} , glucose, and ascorbic acid at 50 mM concentration in 0.1 M TRIS buffer solution (pH 7).

According to the above method, firstly, the 0.1 M TRIS buffer solution (pH 7) was dropped on the surface of AgNPs/GO/SPE sensor for 60 s. After that, 50 mM of Na^+ was added into the solution. The interferences including K^+ , Zn^{2+} , Mg^{2+} , glucose, and ascorbic acid were then sequentially dropped. The percentage recovery was calculated as followed Equation (1):

$$\% \text{ Recovery} = (I_S - I_U)/I_S \times 100 \quad (1)$$

where

I_S = Response current for Na^+ detection (mA)

I_U = Response current for interfering compounds detection (mA)

2.5. Real Sample Analysis

The stock solutions of real samples were prepared from fish sauce and seasoning powder of instant noodles. Firstly, the 0.2 g fish sauce and seasoning powder of instant noodles were dissolved in a beaker containing 25 mL ethanol and sonicated for 1 h. After that, the mixture solutions were filtered via Whatman filter paper for separation any residues. The filtrate was finally diluted to 25 mL with 0.1 M TRIS buffer solution (pH 7) which was used as stock solution for electrochemical analysis.

The standard addition was adopted for determination of Na^+ in real sample. The 0.5 mL of 50 mM NaCl (the standard solution) was spiked into the 0.5 mL stock solutions of fish sauce and seasoning powder of instant noodles. Next, the spiked mixture solution was stirred and mixed with 0.1 M TRIS buffer solution (pH 7). Finally, the origin food samples and the spike samples (origin food samples + 50 mM Na^+) were analyzed via CV method.

3. Results and Discussion

3.1. Characterization of AgNPs/GO Sensing Nanocomposite

Raman spectrum of synthesized GO is displayed in Figure 3a. It exhibits two typical GO peaks with good quality at 1350 and 1577 cm^{-1} that refer to the D and G bands, respectively. The D band is assigned to breathing mode of A_{1g} symmetry involving phonons near edge states and defects (K zone boundary) while the G band is related to the E_{2g} mode of sp^2 -hybridized carbon bond [24,25]. Similar intensity between the D and G peaks indicates the presence of structural disorder from oxygen functional groups corresponding to previous publications [25,26]. UV-Vis spectra of synthesized GO and AgNPs/GO are shown in Figure 3b. The GO (blue line) shows a strong absorption peak at 230 nm and a small shoulder peak at ~ 300 nm corresponding to the π - π^* transitions of aromatic C-C in sp^2

domains and $n-\pi^*$ transitions of C=O and COOH in sp^3 domains, respectively [27–30]. Compared with the spectra of AgNPs, the AgNPs/GO (red line) exhibited a redshift which indicated the successful formation of AgNPs on GO surface [31,32]. Additional peak of AgNPs/GO nanocomposite at 410 nm represented the complete reduction of $AgNO_3$ [33,34] in which the Ag^+ was reduced to metallic Ag. TEM images of AgNPs/GO nanocomposite are shown in Figure 4. The spherical AgNPs are well embedded on the GO surface with an average diameter of 30 nm. The high resolution TEM image (the inset of Figure 4) shows a magnified zone of the selected particles. The D-spacing of the crystal was 0.237 nm corresponding to the AgNPs crystalline in nature [35,36]. The morphologies of AgNPs/GO sensing surfaces before and after 30 cycles of CV measurement with Na^+ are displayed in Figure 5a,b, respectively. After reactions with Na^+ , average diameter of AgNPs decorated on GO becomes significant bigger. This may be correlated to formation and progressive thickening of Na^+ on AgNPs by repeated cycling. However, there is no significant difference in the surface morphology of the AgNPs/GO after 30 cycles of CV measurement with Na^+ . The results refer a good coating of the Na^+ on AgNPs/GO and the stable structure of the AgNPs/GO during the Na^+ intercalation and extraction processes.

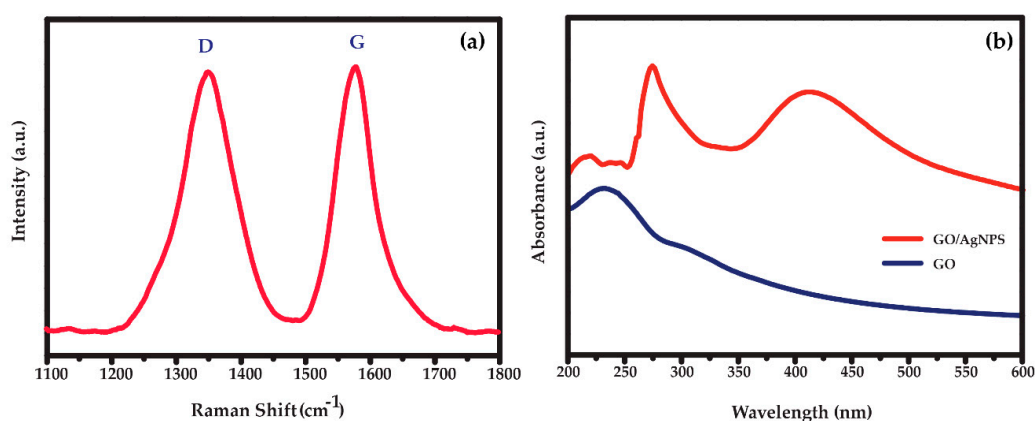


Figure 3. (a) Raman spectra of GO and (b) UV-Vis spectra of the synthesized AgNPs/GO nanocomposite.

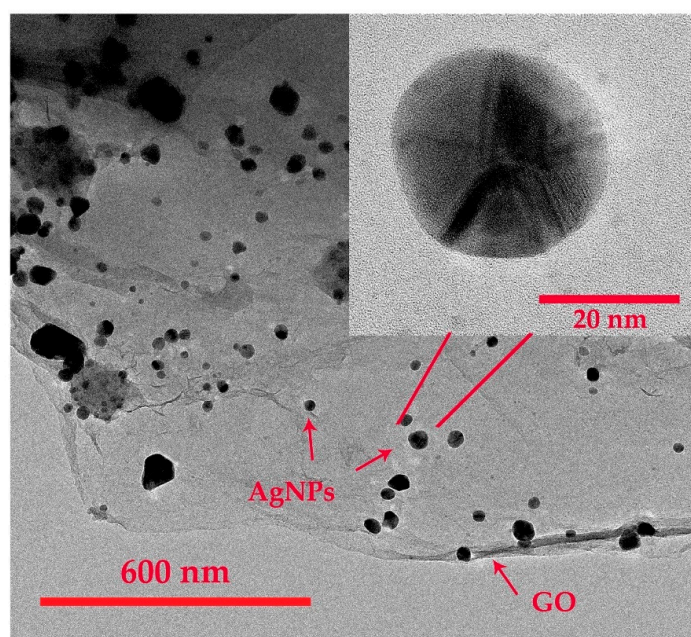


Figure 4. Transmission electron microscopy (TEM) images of the synthesized AgNPs/GO nanocomposite.

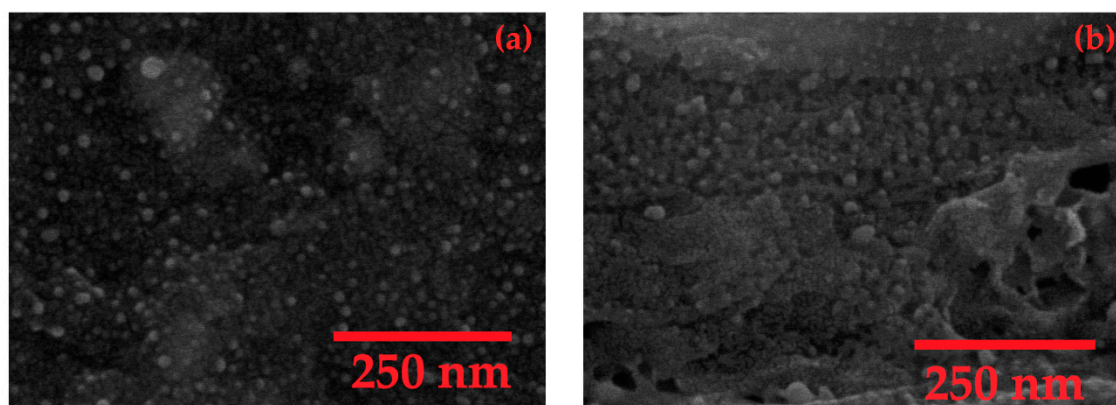


Figure 5. Scanning electron microscope (SEM) images of the synthesized AgNPs/GO nanocomposite (a) before and (b) after 30 cycles of CV measurement with Na⁺.

3.2. Sodium Ion Detection of AgNPs/GO/SPE Sensor

3.2.1. Electrochemical Determination of Na⁺ on AgNPs/GO/SPE Sensor

A relationship between the anodic/cathodic peak currents and the concentration of Na⁺ was investigated by using CV. The AgNPs/GO/SPE sensor was applied a potential range from -1.0 to 1.0 V at a scan rate of 100 mV s^{-1} . Figure 6a shows CVs obtained from different concentrations of standard Na⁺ solution ranging from 0 to 100 mM. The anodic (I_{pa}) and cathodic (I_{pc}) peak currents were presented at $+0.20$ V and -0.35 V on the forward and backward scan, respectively. Both I_{pa} and I_{pc} increased as a function of Na⁺ concentration. The anodic and cathodic peak potential positively shifted as the concentration of Na⁺ increased. The AgNPs/GO showed a well-defined voltammogram with high sensitivity to Na⁺ (current $> 1000 \mu\text{A}$). The I_{pa} and the I_{pc} were approximately equally. These results suggested a reversible process of Na⁺ reaction on AgNPs/GO nanocomposite due to a rapid electron-transfer rate [37]. The peak potential difference ($\Delta E_p = E_{pa} - E_{pc}$) was 0.55 for 30 mM indicating that the redox process is a quasi-reversible system. It should be noted that the potential difference due to ohmic drop effects [38] can be negligible in this study. The linear relationship between I_{pa} and Na⁺ concentration can be expressed as $I_{pa} \text{ (mA)} = 0.019 \times C \text{ (mM)} + 0.865$ with the estimated R^2 values of 0.993 as shown in Figure 6b. It should be noted that the presented I_{pa} is the average value of three independent measurements. In addition, the sensitivity was calculated as 0.269 mA/mM/cm^2 based on Equation (2) [39]. The limit of detection (LOD) was identified as 9.344 mM ($S/N = 3$) followed Equation (3). These results confirmed high sensitivity of AgNPs/GO/SPE sensor for Na⁺ determination with diffusion-controlled kinetics.

$$\text{Sensitivity} = m/A \quad (2)$$

where

m = Slope of calibration plot (mA/mM)

A = Active surface area (cm^2)

$$\text{Detection limit (LOD)} = (3 \times \text{BSD})/N \quad (3)$$

where

BSD = Blank solution standard deviation

N = Slope of calibration plots

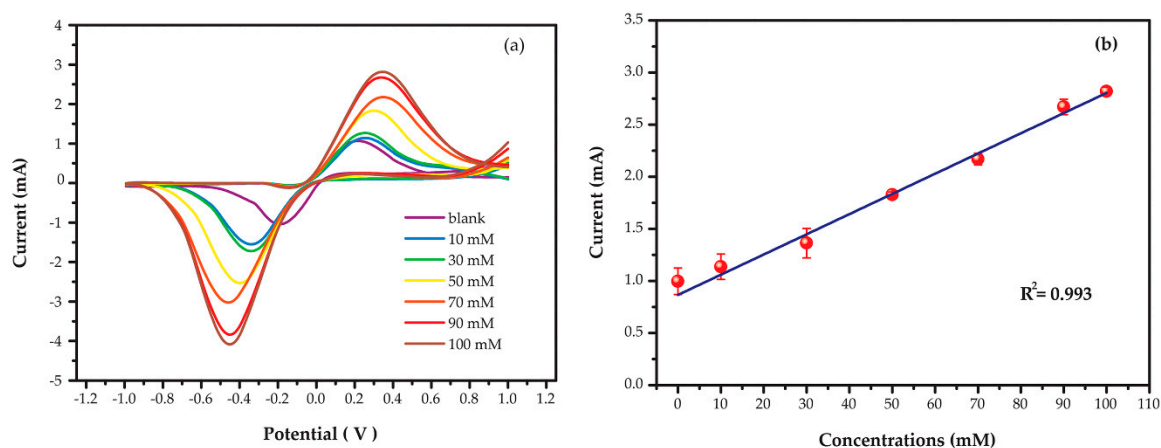


Figure 6. (a) Cyclic voltammograms and (b) relative anodic peak currents of AgNPs/GO/SPE sensors in different sodium concentrations at a scan rate of 100 mV s^{-1} .

3.2.2. Effect of the pH

A study of pH affecting the determination in the pH range of 4.0–10.0 in 0.1 M TRIS solution demonstrated that the anodic peak currents increased with rising pH and reached the maximum at pH 7.0 and dropped afterwards, as shown in Figure 7. The possible reason relies on the reaction of disproportionation and degree of protonation [40,41]. At neutral pH, Na^+ can strongly interact with AgNPs/GO nanocomposite due to surface bound oxide functionalities leading to the highest proton/electron transfer. Thus, the pH 7.0 was chosen as the optimized value for Na^+ determination.

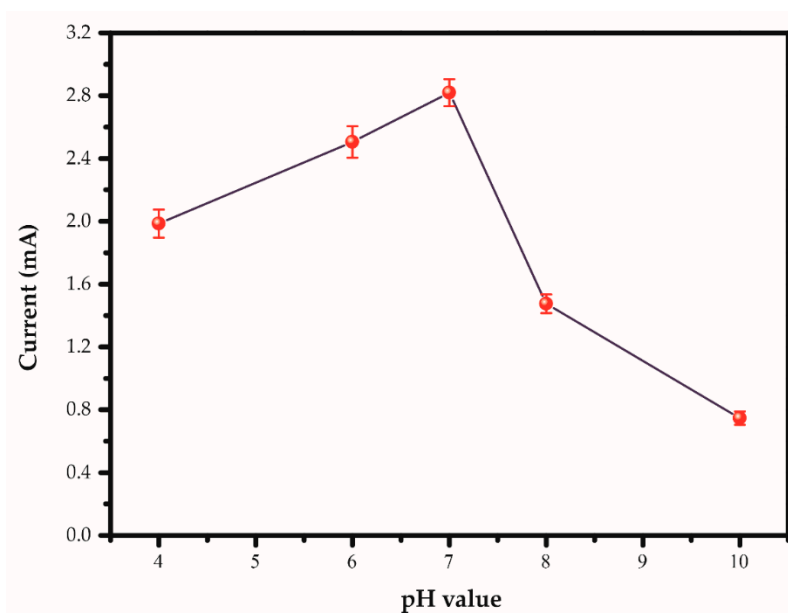


Figure 7. Anodic peak currents of AgNPs/GO/SPE sensor in 100 mM sodium concentration in 0.1 M TRIS at the different pH at a scan rate of 100 mV s^{-1} .

3.2.3. Effect of the Interference

The selectivity is one of the important parameters for practical application. The % recovery based on chronoamperometry in the presence of interfering analytes in food such as K^+ , Zn^{2+} , Na^+ , Mg^{2+} , glucose, and ascorbic acid at 50 mM concentration is shown in Figure 8. The original chronoamperometric current response is displayed in Figure S1 in the Supplementary Information. It should be noted that the response current can be evaluated from chronoamperogram after target sample injection to the peak current as shown in Figure S2 in the Supplementary Information. Although

the background current has not yet stabilized, the response current can be well reproduced based on three sensors measurements. The % recovery can be found in the range of 82.41–90.29% proving that the interfering species did not have any influence on the Na^+ determination and the AgNPs/GO was very selective to Na^+ . The prepared electrode was therefore suitable for quantitative determination of Na^+ . In general, K^+ can interact with sensing materials via ion exchange in the same manner of Na^+ . However, Na^+ owns the smaller ionic radius compared with the K^+ in which it easily inserts into the AgNPs/GO nanocomposite and makes strong interactions on sensing composites resulting in less available on bigger ionic radius to adsorb on AgNPs/GO nanocomposite.

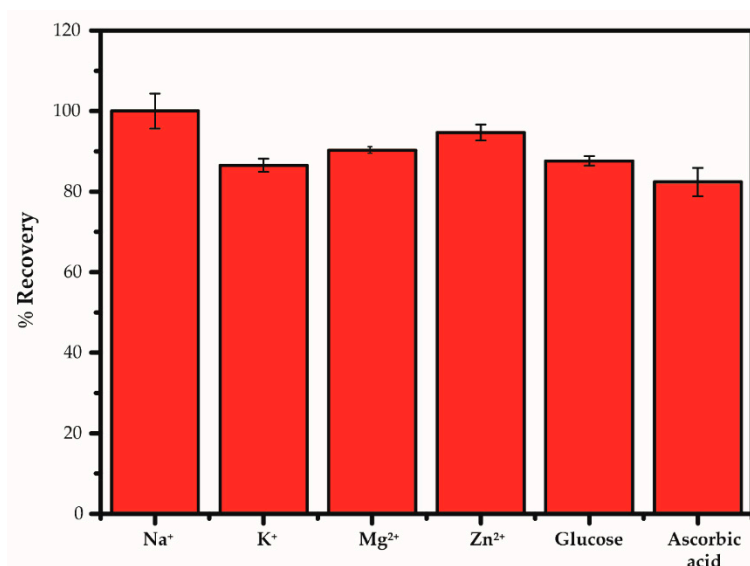


Figure 8. Comparisons of interfering substances added into 50 mM sodium under the optimized conditions of measurement by using the AgNPs/GO/SPE sensors based on chronoamperometry.

3.2.4. Reproducibility, Repeatability, and Stability of AgNPs/GO/SPE Sensor

To confirm the precision of the proposed AgNPs/GO/SPE sensor, the reproducibility, repeatability and stability of AgNPs/GO/SPE sensors were examined. The pattern of CV for 250 mM Na^+ exhibits the similar behavior from cycle 1 to cycle 10 as shown in Figure 9a. The peak potential and peak current increase a bit between first cycle and tenth cycle. This shift comes from accumulation of charges and normal electrochemical activity in sensing film. At the first cycling, it is an initial phase for oxidation and reduction reactions. After the seventh cycling, the initial phase undergoes a transformation towards more stable phase. The five electrodes prepared from the same procedure were used to determine 250 mM Na^+ in 0.1 M TRIS (pH = 7.0). The average anodic peak current calculated from last three cycles of each electrode is displayed in Figure 9b. The original CVs of each electrode (electrodes 2–5) are displayed in Figure S3 in the Supplementary Information. No obvious fluctuation of peak currents can be found from all fabricated AgNPs/GO/SPE sensors for 250 mM Na^+ detection. The relative standard deviation (RSD) were approximately 4.6% only. After drop coating of sensing films on electrodes, the sensors were kept at room temperature (26 ± 2 °C). The I_{pa} of AgNPs/GO/SPE sensors for 250 mM Na^+ detection was monitored after one month and found to be reproducible responses with no significant change in CV pattern. These results indicate the excellent reproducibility, repeatability and stability of AgNPs/GO/SPE sensors.

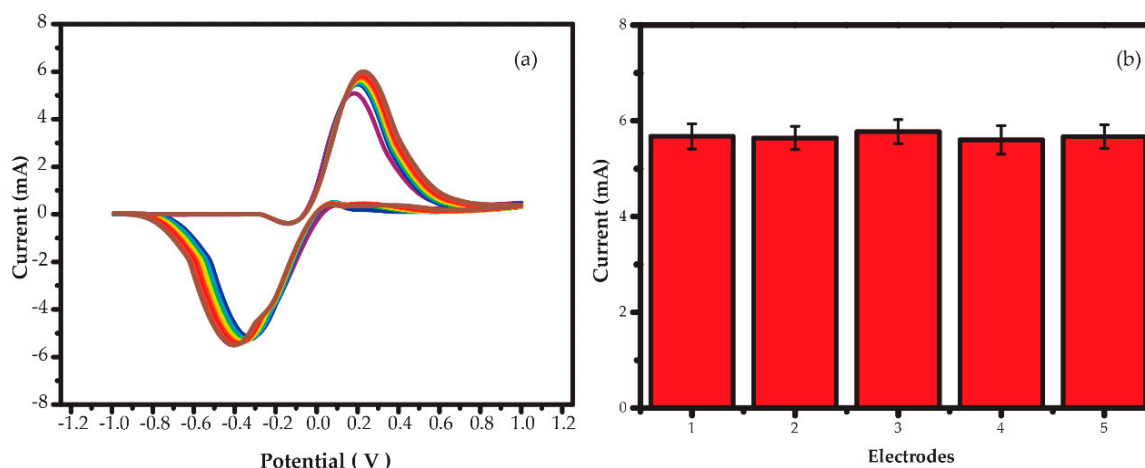


Figure 9. (a) Cyclic voltammograms as a function of the number of cycles and (b) plot of the anodic peak current of five AgNPs/GO/SPE sensors at a scan rate of 100 mV s^{-1} .

3.2.5. Electrochemical Analysis of Real Samples

Na^+ in real samples such as fish sauce and seasoning powder of instant noodles were also successfully determined by using the AgNPs/GO/SPE sensors. The CVs and relative anodic peak currents of real samples and spiked samples (real samples +50 mM Na^+) are displayed in Figure S4 in the Supplementary Information. Measurement results of non-spiked and spiked samples are summarized in Table 1. The results for Na^+ determination in real samples of fish sauce and seasoning powder of instant noodles were satisfactory with the recovery of 100.80% and 94.48%, respectively. Triplicate analysis of the samples was achieved with the reasonably good RSDs of between 1.03 and 1.22%. The results confirmed a potential application of the AgNPs/GO/SPE for determination of Na^+ in real samples. It should be noted that concentration of Na^+ in the real samples and spiked samples was calculated from calibration curve (Figure 6b) and the percentage recovery for real sample testing was evaluated via Equation (4):

$$\% \text{ Recovery} = (C_F - C_O)/C_A \times 100 \quad (4)$$

where

C_F = Concentration of Na^+ in spiked sample (mM)

C_O = Concentration of original Na^+ in real sample (mM)

C_A = Concentration of added Na^+ in real sample (mM)

Table 1. Determination of sodium in real sample.

Samples	Original (C_O) (mM)	Added (C_A) (mM)	Found (C_F) (mM)	Recovery (%)	RSD (%)
Fish sauce	77.75	50.00	128.15	100.80	1.03
Seasoning powder of instant noodle	48.30	50.00	95.54	94.48	1.22

3.2.6. Sensing Mechanism

Based on the results, the possible mechanism of the AgNPs/GO/SPE using the CV technique may be explained by oxidation/reduction reactions of the AgNPs/GO/SPE sensor with departure/intercalation of the Na^+ [42]. In an aqueous solution, water molecules dissociate to form hydrogen and hydroxyl ions that can be adsorbed onto a majority of the metal oxide [43]. The Na^+ diffuses into the AgNPs/GO and interact via ion-exchange reactions with both positive and negative going sweeps (reversible process according to CV results from Figures 6a and 9a). At AgNPs/GO/SPE surfaces, they donate/accept a

proton from the solution to form a negative and positive surface group, respectively. Thus, the electric field can be occurred by the charge surface at electrode accumulated in the layer.

Commonly, it is well known that the decoration of AgNPs on surface of GO enhances the catalytic activity leading to the increases of electrode surface area and active sites for capture electron in solution. The GO also owns π - π stacking interaction which induces facile electron transfer between GO and target analytes [44]. Therefore, AgNPs/GO is negatively charged at neutral and basic solutions. In this case, the NaCl dissolves in water, it dissociates completely in to Na^+ and Cl^- . When Na^+ ion was adsorbed onto surface AgNPs/GO occurring charge transfer from Na^+ which acts as donors to the AgNPs/GO leading to increase I_{pa} with increase of Na^+ concentration [45,46].

4. Conclusions

In summary, the AgNPs/GO nanocomposite modified on a screen-printed silver electrode can be successfully used for detecting Na^+ at room temperature because the synergies of GO and AgNPs enhance catalytic performance. The AgNPs were synthesized via an eco-friendly approach at room temperature using *Pistia stratiotes* extract as the reducing agent without any stabilizer. The spherical AgNPs with an average diameter of 30 nm were decorated on GO surfaces and used as high sensing working electrode to Na^+ . The electrochemical behavior of AgNPs/GO/SPE sensor exhibits high sensing performances such as a good linear relationship between anodic peak current and Na^+ concentrations in the range of 0–100 mM ($R^2 = 0.993$), high sensitivity of 0.269 mA/mM/cm², low detection limit of 9.344 mM, less effect on food taste interference analytes, and long stability over one month. With real samples such as fish sauce and seasoning powder of instant noodle, the percentage recovery of AgNPs/GO/SPE sensor for Na^+ detection was in the range of 94%–101%. The remarkable analytical sensitivity of the AgNPs/GO/SPE together with its simple preparation and more economical device makes such the thin-film electrode having a great potential application as a Na^+ sensor for testing the salinity in commercial food products. The further advantage of the Ag NPs/GO/SPE was then its single-use which eliminated the fouling problem of the electrode surface. Based on the results, it is believed that the AgNPs/GO/SPE successfully performed for determination of Na^+ contents in food applications.

Supplementary Materials: The following are available online at <http://www.mdpi.com/2227-9040/8/3/58/s1>, Figure S1: Chronoamperometric current response of AgNPs/GO/SPE sensor for addition of Na^+ in presence of potential food interfering species at a constant potential of + 0.2 V, Figure S2. Chronoamperometric current response of three independent AgNPs/GO/SPE sensors before and after Na^+ injection at a constant potential of + 0.2 V, Figure S3. Cyclic voltammograms of four independent AgNPs/GO/SPE sensors as a function of the number of cycles, Figure S4. Cyclic voltammograms of AgNPs/GO/SPE sensors in (a) real samples and (b) spiked samples (real samples with addition of 50 mM Na^+). The insets show the relative anodic peak currents of AgNPs/GO/SPE sensors.

Author Contributions: Conceptualization, C.W.; methodology, P.T. and C.W.; validation, W.S. and C.W.; formal analysis, P.T., W.S., and C.W.; investigation, P.T. and C.W.; resources, W.S. and C.W.; data curation, P.T. and C.W.; writing—original draft preparation, P.T.; writing—review and editing, C.W.; visualization, P.T.; supervision, C.W.; funding acquisition, W.S. and C.W. All authors have read and agreed to the published version of the manuscript.

Funding: This work was financially supported by Kasetsart University Research and Development Institute (KURDI).

Acknowledgments: P.T. acknowledges the Graduate Program Scholarship from the Graduate School, Kasetsart University.

Conflicts of Interest: The authors declare no conflict of interest.

References

1. Strazzullo, P.; Leclercq, C. Sodium. *Adv. Nutr.* **2014**, *5*, 188–190. [CrossRef] [PubMed]
2. Cutler, J.A.; Follmann, D.; Allender, P.S. Randomized trials of sodium reduction: An overview. *Am. J. Clin. Nutr.* **1997**, *65*, 643S–651S. [CrossRef] [PubMed]

3. Canzanello, V.J.; Sheps, S.G. The Sixth Report of the Joint National Committee on Prevention, Detection, Evaluation, and Treatment of High Blood Pressure: What's New? What's Different? *Cardiol. Rev.* **1998**, *6*, 272–277. [[CrossRef](#)]
4. Galletti, F.; Agabiti-Rosei, E.; Bernini, G.; Boero, R.; Desideri, G.; Fallo, F.; Mallamaci, F.; Morganti, A.; Castellano, M.; Nazzaro, P.; et al. Excess dietary sodium and inadequate potassium intake by hypertensive patients in Italy: Results of the MINISAL-SIIA study program. *J. Hypertens.* **2014**, *32*, 48–56. [[CrossRef](#)] [[PubMed](#)]
5. Villani, A.M.; Clifton, P.M.; Keogh, J.B. Sodium intake and excretion in individuals with type 2 diabetes mellitus: A cross-sectional analysis of overweight and obese males and females in Australia. *J. Hum. Nutr. Diet.* **2012**, *25*, 129–139. [[CrossRef](#)] [[PubMed](#)]
6. Smyth, A.; O'Donnell, M.; Mente, A.; Yusuf, S. Dietary Sodium and Cardiovascular Disease. *Curr. Hypertens. Rep.* **2015**, *17*, 47. [[CrossRef](#)]
7. Sacks, F.M.; Svetkey, L.P.; Vollmer, W.M.; Appel, L.J.; Bray, G.A.; Harsha, D.; Obarzanek, E.; Conlin, P.R.; Miller, E.R.; Simons-Morton, D.G.; et al. Effects on Blood Pressure of Reduced Dietary Sodium and the Dietary Approaches to Stop Hypertension (DASH) Diet. *N. Engl. J. Med.* **2001**, *344*, 3–10. [[CrossRef](#)]
8. Lim, S.S.; Vos, T.; Flaxman, A.D.; Danaei, G.; Shibuya, K.; Adair-Rohani, H.; AlMazroa, M.A.; Amann, M.; Anderson, H.R.; Andrews, K.G.; et al. A comparative risk assessment of burden of disease and injury attributable to 67 risk factors and risk factor clusters in 21 regions, 1990–2010: A systematic analysis for the Global Burden of Disease Study 2010. *Lancet* **2012**, *380*, 2224–2260. [[CrossRef](#)]
9. Tischer, B.; Teixeira, I.D.; Filoda, P.F.; Alessio, K.O.; Barin, J.S.; Duarte, F.A.; Kipper, L.M.; Helfer, G.A.; Costa, A.B.D. Infrared enthalpymetric methods: A new, fast and simple alternative for sodium determination in food sauces. *Food Chem.* **2020**, *305*, 125456. [[CrossRef](#)]
10. Midey, A.J.; Camacho, A.; Sampathkumaran, J.; Krueger, C.A.; Osgood, M.A.; Wu, C. High-performance ion mobility spectrometry with direct electrospray ionization (ESI-HPIMS) for the detection of additives and contaminants in food. *Anal. Chim. Acta* **2013**, *804*, 197–206. [[CrossRef](#)]
11. Garcia-Cordero, E.; Bellando, F.; Zhang, J.; Wildhaber, F.; Longo, J.; Guérin, H.; Ionescu, A.M. Three-Dimensional Integrated Ultra-Low-Volume Passive Microfluidics with Ion-Sensitive Field-Effect Transistors for Multiparameter Wearable Sweat Analyzers. *ACS Nano* **2018**, *12*, 12646–12656. [[CrossRef](#)]
12. Lu, T.-F.; Yang, C.-M.; Wang, J.-C.; Ho, K.-I.; Chin, C.-H.; Pijanowska, D.G.; Jaroszewicz, B.; Lai, C.-S. Characterization of K⁺ and Na⁺-Sensitive Membrane Fabricated by CF₄ Plasma Treatment on Hafnium Oxide Thin Films on ISFET. *J. Electrochem. Soc.* **2011**, *158*, J91. [[CrossRef](#)]
13. Cazalé, A.; Sant, W.; Launay, J.; Ginot, F.; Temple-Boyer, P. Study of field effect transistors for the sodium ion detection using fluoropolysiloxane-based sensitive layers. *Sens. Actuators B Chem.* **2013**, *177*, 515–521. [[CrossRef](#)]
14. Zhang, J.; Rupakula, M.; Bellando, F.; Garcia Cordero, E.; Longo, J.; Wildhaber, F.; Herment, G.; Guérin, H.; Ionescu, A.M. Sweat Biomarker Sensor Incorporating Picowatt, Three-Dimensional Extended Metal Gate Ion Sensitive Field Effect Transistors. *ACS Sens.* **2019**, *4*, 2039–2047. [[CrossRef](#)] [[PubMed](#)]
15. Manikandan, V.S.; Adhikari, B.; Chen, A. Nanomaterial based electrochemical sensors for the safety and quality control of food and beverages. *Analyst* **2018**, *143*, 4537–4554. [[CrossRef](#)]
16. Zahed, F.M.; Hatamluyi, B.; Lorestani, F.; Es'haghi, Z. Silver nanoparticles decorated polyaniline nanocomposite based electrochemical sensor for the determination of anticancer drug 5-fluorouracil. *J. Pharm. Biomed. Anal.* **2018**, *161*, 12–19. [[CrossRef](#)]
17. Traiwatcharanon, P.; Timsorn, K.; Wongchoosuk, C. Flexible room-temperature resistive humidity sensor based on silver nanoparticles. *Mater. Res. Express* **2017**, *4*, 085038. [[CrossRef](#)]
18. Huang, X.-M.; Liu, L.-Z.; Zhou, S.; Zhao, J.-J. Physical properties and device applications of graphene oxide. *Front. Phys.* **2020**, *15*, 33301. [[CrossRef](#)]
19. Seekaew, Y.; Pon-On, W.; Wongchoosuk, C. Ultrahigh Selective Room-Temperature Ammonia Gas Sensor Based on Tin–Titanium Dioxide/reduced Graphene/Carbon Nanotube Nanocomposites by the Solvothermal Method. *ACS Omega* **2019**, *4*, 16916–16924. [[CrossRef](#)]
20. Arunragasa, S.; Seekaew, Y.; Pon-On, W.; Wongchoosuk, C. Hydroxyl edge-functionalized graphene quantum dots for gas-sensing applications. *Diam. Relat. Mater.* **2020**, *105*, 107790. [[CrossRef](#)]
21. Seekaew, Y.; Wongchoosuk, C. A novel graphene-based electroluminescent gas sensor for carbon dioxide detection. *Appl. Surf. Sci.* **2019**, *479*, 525–531. [[CrossRef](#)]

22. Seekaew, Y.; Wisitsoraat, A.; Phokharatkul, D.; Wongchoosuk, C. Room temperature toluene gas sensor based on TiO₂ nanoparticles decorated 3D graphene-carbon nanotube nanostructures. *Sens. Actuators B Chem.* **2019**, *279*, 69–78. [[CrossRef](#)]
23. Seekaew, Y.; Phokharatkul, D.; Wisitsoraat, A.; Wongchoosuk, C. Highly sensitive and selective room-temperature NO₂ gas sensor based on bilayer transferred chemical vapor deposited graphene. *Appl. Surf. Sci.* **2017**, *404*, 357–363. [[CrossRef](#)]
24. Spilarewicz-Stanek, K.; Kisielewska, A.; Ginter, J.; Bałuszyńska, K.; Piwoński, I. Elucidation of the function of oxygen moieties on graphene oxide and reduced graphene oxide in the nucleation and growth of silver nanoparticles. *RSC Adv.* **2016**, *6*, 60056–60067. [[CrossRef](#)]
25. Gutić, S.; Dobrota, A.; Gavrilov, N.; Baljovic, M.; Pasti, I.; Mentus, S. Surface Charge Storage Properties of Selected Graphene Samples in pH-neutral Aqueous Solutions of Alkali Metal Chlorides-Particularities and Universalities. *Int. J. Electrochem. Sci.* **2016**, *11*, 8662–8682. [[CrossRef](#)]
26. Gutić, S.J.; Dobrota, A.S.; Leetmaa, M.; Skorodumova, N.V.; Mentus, S.V.; Pašti, I.A. Improved catalysts for hydrogen evolution reaction in alkaline solutions through the electrochemical formation of nickel-reduced graphene oxide interface. *Phys. Chem. Chem. Phys.* **2017**, *19*, 13281–13293. [[CrossRef](#)] [[PubMed](#)]
27. Li, S.-S.; Hu, Y.-Y.; Feng, J.-J.; Lv, Z.-Y.; Chen, J.-R.; Wang, A.-J. Rapid room-temperature synthesis of Pd nanodendrites on reduced graphene oxide for catalytic oxidation of ethylene glycol and glycerol. *Int. J. Hydrogen Energy* **2014**, *39*, 3730–3738. [[CrossRef](#)]
28. Bhargava, R.; Khan, S.; Ansari, M.M.N.; Ahmad, N. Green synthesis approach for the reduction of graphene oxide by using glucose. *AIP Conf. Proc.* **2019**, *2115*, 030075. [[CrossRef](#)]
29. Sunderrajan, S.; Miranda, L.R.; Pennathur, G. Improved stability and catalytic activity of graphene oxide/chitosan hybrid beads loaded with porcine liver esterase. *Prep. Biochem. Biotechnol.* **2018**, *48*, 343–351. [[CrossRef](#)]
30. Cobos, M.; De-La-Pinta, I.; Quindós, G.; Fernández, M.J.; Fernández, M.D. Graphene Oxide-Silver Nanoparticle Nanohybrids: Synthesis, Characterization, and Antimicrobial Properties. *Nanomaterials (Basel)* **2020**, *10*, 376. [[CrossRef](#)]
31. Kumari, S.; Sharma, P.; Yadav, S.; Kumar, J.; Vij, A.; Rawat, P.; Kumar, S.; Sinha, C.; Bhattacharya, J.; Srivastava, C.M.; et al. A Novel Synthesis of the Graphene Oxide-Silver (GO-Ag) Nanocomposite for Unique Physiochemical Applications. *ACS Omega* **2020**, *5*, 5041–5047. [[CrossRef](#)] [[PubMed](#)]
32. Khorrami, S.; Abdollahi, Z.; Eshaghi, G.; Khosravi, A.; Bidram, E.; Zarrabi, A. An Improved Method for Fabrication of Ag-GO Nanocomposite with Controlled Anti-Cancer and Anti-bacterial Behavior; A Comparative Study. *Sci. Rep.* **2019**, *9*, 9167. [[CrossRef](#)] [[PubMed](#)]
33. Mohammadi, F.; Yousefi, M.; Ghahremanzadeh, R. Green synthesis, characterization and antimicrobial activity of silver nanoparticles (AgNPs) using leaves and stems extract of some plants. *Adv. J. Chem. Sect. A* **2019**, *2*, 266–275. [[CrossRef](#)]
34. Zhang, Y.; Liu, S.; Wang, L.; Qin, X.; Tian, J.; Lu, W.; Chang, G.; Sun, X. One-pot green synthesis of Ag nanoparticles-graphene nanocomposites and their applications in SERS, H₂O₂, and glucose sensing. *RSC Adv.* **2012**, *2*, 538–545. [[CrossRef](#)]
35. Jayanthi, M.; Megarajan, S.; Subramaniyan, S.B.; Kamlekar, R.K.; Veerappan, A. A convenient green method to synthesize luminescent carbon dots from edible carrot and its application in bioimaging and preparation of nanocatalyst. *J. Mol. Liq.* **2019**, *278*, 175–182. [[CrossRef](#)]
36. Some, S.; Bulut, O.; Biswas, K.; Kumar, A.; Roy, A.; Sen, I.K.; Mandal, A.; Franco, O.L.; Ince, İ.A.; Neog, K.; et al. Effect of feed supplementation with biosynthesized silver nanoparticles using leaf extract of *Morus indica* L. V1 on *Bombyx mori* L. (Lepidoptera: Bombycidae). *Sci. Rep.* **2019**, *9*, 14839. [[CrossRef](#)]
37. Manikandan, V.S.; Sidhureddy, B.; Thirupathi, A.R.; Chen, A. Sensitive Electrochemical Detection of Caffeic Acid in Wine Based on Fluorine-Doped Graphene Oxide. *Sensors (Basel)* **2019**, *19*, 1604. [[CrossRef](#)]
38. Elgrishi, N.; Rountree, K.J.; McCarthy, B.D.; Rountree, E.S.; Eisenhart, T.T.; Dempsey, J.L. A Practical Beginner's Guide to Cyclic Voltammetry. *J. Chem. Educ.* **2018**, *95*, 197–206. [[CrossRef](#)]
39. Balakrishnan, S.R.; Hashim, U.; Gopinath, S.C.; Poopalan, P.; Ramayya, H.R.; Iqbal Omar, M.; Haarindraprasad, R.; Veeradasan, P. A Point-of-Care Immunosensor for Human Chorionic Gonadotropin in Clinical Urine Samples Using a Cuneated Polysilicon Nanogap Lab-on-Chip. *PLoS ONE* **2015**, *10*, e0137891. [[CrossRef](#)]

40. Machini, W.B.S.; Martin, C.S.; Martinez, M.T.; Teixeira, S.R.; Gomes, H.M.; Teixeira, M.F.S. Development of an electrochemical sensor based on nanostructured hausmannite-type manganese oxide for detection of sodium ions. *Sens. Actuators B Chem.* **2013**, *181*, 674–680. [[CrossRef](#)]
41. Runnels, P.L.; Joseph, J.D.; Logman, M.J.; Wightman, R.M. Effect of pH and Surface Functionalities on the Cyclic Voltammetric Responses of Carbon-Fiber Microelectrodes. *Anal. Chem.* **1999**, *71*, 2782–2789. [[CrossRef](#)] [[PubMed](#)]
42. Kanoh, H.; Tang, W.; Makita, Y.; Ooi, K. Electrochemical Intercalation of Alkali-Metal Ions into Birnessite-Type Manganese Oxide in Aqueous Solution. *Langmuir* **1997**, *13*, 6845–6849. [[CrossRef](#)]
43. Abbar, A.H.; Abbas, A.S. A Kinetic Study of Oxalic Acid Electrochemical Oxidation on a Manganese Dioxide Rotating Cylinder Anode. *Port. Electrochim. Acta* **2018**, *36*, 325–337. [[CrossRef](#)]
44. Lee, C.-S.; Yu, S.H.; Kim, T.H. One-Step Electrochemical Fabrication of Reduced Graphene Oxide/Gold Nanoparticles Nanocomposite-Modified Electrode for Simultaneous Detection of Dopamine, Ascorbic Acid, and Uric Acid. *Nanomaterials* **2018**, *8*, 17. [[CrossRef](#)]
45. Moon, H.; Lee, J.; Kwon, S.; Kim, I.T.; Lee, S.G. Mechanisms of Na adsorption on graphene and graphene oxide: Density functional theory approach. *Carbon Lett.* **2015**, *16*, 116–120. [[CrossRef](#)]
46. Jeong, S.Y.; Kim, S.H.; Han, J.T.; Jeong, H.J.; Jeong, S.Y.; Lee, G.-W. Highly Concentrated and Conductive Reduced Graphene Oxide Nanosheets by Monovalent Cation- π Interaction: Toward Printed Electronics. *Adv. Funct. Mater.* **2012**, *22*, 3307–3314. [[CrossRef](#)]



© 2020 by the authors. Licensee MDPI, Basel, Switzerland. This article is an open access article distributed under the terms and conditions of the Creative Commons Attribution (CC BY) license (<http://creativecommons.org/licenses/by/4.0/>).